Inorganic Chemistry Communications 125 (2021) 108430

Contents lists available at ScienceDirect

Inorganic Chemistry Communications

journal homepage: www.elsevier.com/locate/inoche

Short communication

pH-responsive and CD44-targeting by Fe_3O_4/MSNs-NH_2 nanocarriers for Oxaliplatin loading and colon cancer treatment

Hamed Tabasi [a,b], M.T. Hamed Mosavian [a], Zahra Sabouri [c], Majid Khazaei [d], Majid Darroudi [e,f,*]

[a] Department of Chemical Engineering, Faculty of Engineering, Ferdowsi University of Mashhad, Mashhad, Iran
[b] Pharmaceutical Research Center, Pharmaceutical Technology Institute, Mashhad University of Medical Sciences, Mashhad, Iran
[c] Neurogenic Inflammation Research Center, Mashhad University of Medical Sciences, Mashhad, Iran
[d] Department of Medical Biotechnology and Nanotechnology, Faculty of Medicine, Mashhad University of Medical Sciences, Mashhad, Iran
[e] Nuclear Medicine Research Center, Mashhad University of Medical Sciences, Mashhad, Iran
[f] Department of Medical Biotechnology & Nanotechnology, Faculty of Medicine, Mashhad University of Medical Sciences, Mashhad, Iran

ARTICLE INFO

Keywords:
Fe_3O_4
MSNs
HCT-116
Colon cancer
CD-44 receptor
NH_2-bonding

ABSTRACT

In this work, we have introduced a promising method for performing colon HCT-116 cancer cells treatment by the usage of CD44 to function as the targeting receptors. For this purpose, we have synthesized super-paramagnetic Fe_3O_4/Mesoporous silica nanoparticles (MSNs) through co-precipitation and sol–gel process and had the surface of the obtained nanocarriers (NCs) functionalized by NH_2-bonding. The functionalized NCs have been characterized by the means of FT-IR spectroscopy, VSM, TEM, and FE-SEM. In the following, the values of drug loading and release have been measured through the application of ICP-OES analysis for 48 h, in which the drug release profile has been studied in both human blood (pH 7.4) and cancer cell (pH 5.0) conditions. According to the final results of MTT assay, the IC_{50} of Free drug and NCs -drug loaded has faced a decrease, from 7.5 μg/mL to 3.2 μg/mL, due to the fact that NH_2 had been able to express a higher Oxaliplatin intracellular uptake and more CD44-binding than free Oxaliplatin. Therefore, this work has attempted to highlight these Fe_3O_4/MSNs-NH_2 NCs potential in standing as a superior candidate for Oxaliplatin loading and colon cancer treatment.

1. Introduction

Nowadays, cancer is known as a fast-growing cause of death throughout the world since there are different types of cancer cells including colon cancer, breast cancer, skin cancer, bone cancer, head and neck cancer, and prostate cancer [1–3]. Considering how chemotherapy can engage most of the normal cells and cause excessively high toxic side effects, such as kidney toxicity, hearing impairment, nausea, hair loss, and bone marrow suppression, however performing cancer therapy with the usage of NCs can eliminate the toxicity of drugs and reduce the negative impacts even down to zero [4–8]. Fe_3O_4 NPs have been widely used as-decorated (or without shell) NPs utilizing in different nano-biomedicine applications [9] such as biological separation (DNA/ protein/ heavy metal) [10–18], magnetic resonance imaging (MRI) [19,20], hyperthermia [21,22], and drug delivery. several researchers decorated the mineral Fe_3O_4 with a thin layer of organic/ inorganic agents as SiO_2 [23], SiO_3 [11], Chitosan [24], Au [25], and Ag [26] in order to prepare the core–shell system with interesting super-paramagnetic properties as antimicrobial [27,28], antibacterial [29,30], antioxidant [31–33], antifungal, and anticancer activities [34–37]. Silica-based nanocarriers have been becoming increasingly popular due to its biocompatibility, chemical & physical stability, surface-functionable, tunable-structure, simple and economic experimental processes [38,39].

Among the available chemotherapeutic agents, platinum anticancer drugs, including cisplatin, carboplatin, and Oxaliplatin (OXA), have proved to be capable of treating about 40–80% of all cancer patients. In addition, nedaplatin, lobaplatin, and heptaplatin stand as the regional forms of Pt (II) drugs [40,41]. Fig. 1 illustrates the different types of platinum anticancer drugs.

OXA (acid oxalate – platinum (II)) is the third generation of Pt (II) that is able to reduce the side effects of cisplatin and overcome its resistance. Although this substance contains lower toxicity when compared to the kidneys and bone marrow, yet it has displayed higher

* Corresponding author at: Nuclear Medicine Research Center, Mashhad University of Medical Sciences, Mashhad, Iran.
E-mail address: darroudim@mums.ac.ir (M. Darroudi).

https://doi.org/10.1016/j.inoche.2020.108430
Received 17 September 2020; Received in revised form 22 December 2020; Accepted 23 December 2020
Available online 29 December 2020

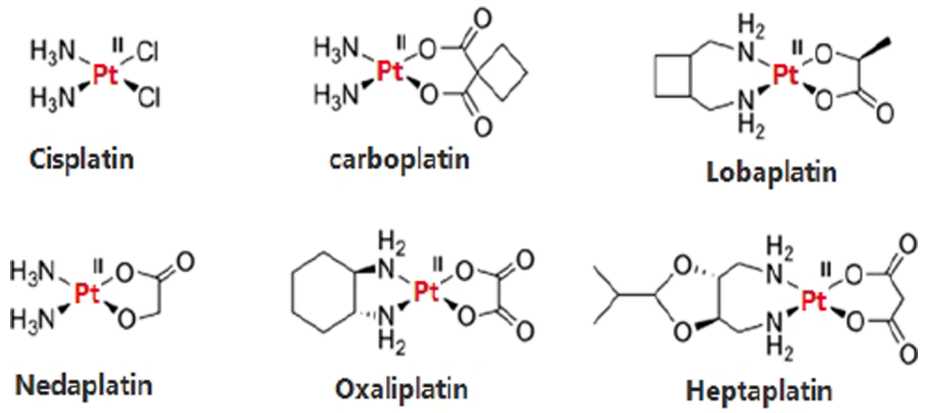

Fig. 1. Different structures of Pt (II) drugs.

toxicity towards colon cancer in contrast to the other Pt drugs [42]. Furthermore, the structure–activity of OXA, 1,2-diaminocyclohexane (DACH) has been reported to be more stable, which is fabricated as the oxalic acid ligand leaves the OXA molecule [43]. Every cell cancer contains a particular receptor that can be detected by external NCs, for which the HCT-116 colon cancer cells could be stated as a suitable example. According to the several kinds of research that had targeted the CD-44 receptors of this type of cancer cells [44–46], the NCs that had been altered through hyaluronic acid modification have been able to detect these receptors with increased efficacy [16–18]. However, in this work, the surface of Fe_3O_4/MSNs have been functionalized by the utilization of NH_2-groups to increase their stability and dispersity for achieving a higher drug loading. In comparison to the proportion of free drugs, the obtained modified NCs have exhibited more efficacy on cancer cells and higher stability in human blood condition (pH: 7.4), which can be applied for carrying drugs to the targeted cancer cells without the occurrence of any releasing.

2. Experimental section

2.1. Materials

Ferrous chloride ($FeCl_2{\cdot}4H_2O$, $\geq$ 99.7%), ferric chloride hexahydrate ($FeCl_3{\cdot}6H_2O$, $\geq$99.7%), Cetyl trimethylammonium bromide (CTAB), tetraethyl orthosilicate (TEOS) (98%), hydrochloric acid (HCl, 37%), sodium hydroxide (NaOH), ethanol (99.6%), and 5-diphenyl tetrazolium bromide (MTT), as well as acetate buffer solution (ABS) at the pH of 5.0 and phosphate buffer solution (PBS) at the pH of 7.4, have been purchased from Sigma-Aldrich. We have also procured 3-Aminopropyltriethoxysilane (APTES), Cell culture medium Dulbecco's modified eagle medium (DMEM), penicillin, streptomycin, OXA, and HCT-116 cells from Merck (Germany). All of the involved solutions have been prepared through the usage of ultra-pure water.

2.2. Preparation of nanocarriers

The required magnetic NPs have been prepared by co-precipitation. After being synthesized, the Fe_3O_4 NPs have been encapsulated with MSNs through a sol–gel method. Briefly, $FeCl_2{\cdot}4H_2O$ and $FeCl_3{\cdot}6H_2O$ with the molar proportion of 1:3 have been dissolved in 12.5 mL of water that contained 0.6 mL of HCl (37% v/v) under vigorous magnetic stirring in a nitrogen atmosphere. The temperature of the solution has been slowly increased to 80 °C while being stirred for 1 h and once the solution had been cooled down to room temperature, 20 mL of NaOH (97%) has been added drop wisely throughout half an hour. Thereafter, the temperature of the mixture has been heightened to 80 °C one more round and kept for 30 min. The obtained black precipitates have been collected with a magnet and washed several times with water and ethanol. In the following, the as-prepared Fe_3O_4 NPs have been encapsulated by MSNs in an aquase solution, which had contained CTAB and lacked the presence of any linker between Fe_3O_4 surface and CTAB by performing the aging process. As the last step, the as-synthesized NCs have been functionalized by the application of NH_2-group in ethanol solvent. Typically, we have dispersed the synthesized Fe_3O_4/MSNs (0.15 g) in ethanol (15 mL) by being sonicated for 30 min and afterwards, had the APTES (200 μL) quickly added and stirred for 24 h at room temperature. The obtained Fe_3O_4/MSN-NH_2 has been washed with ethanol and separated by an external magnet to being dried.

2.3. Drug loading

Initially, Fe_3O_4/MSN and Fe_3O_4/MSNs-NH_2 have been dispersed in two separate mixtures including 6.7 mL of water and 3.3 mL of OXA (5 mg/mL). Thereafter, the solutions have been sonicated for 5 min at 45 °C and left under stirring in darkness for 48 h at room temperature. Eventually, the NCs have been separated by the usage of an external magnet, washed several times for removing adsorbed-drug, and dried under vacuum.

2.4. In vitro drug release

In order to investigate the OXA release profile at varying time intervals, 1 mg drug-loaded of Fe_3O_4/MSNs-NH_2 has been re-dispersed in two separate conditions of ABS with pH of 5.0 (cell cancer situation) and PBS with pH of 7.4 (human blood situation). The suspensions were transferred into a dialysis bag (MWCO = 3500) and incubated at 37 °C. In addition, the ICP-OES method has been applied to measure the amount of drug release subsequent to 3, 6, 12, 24, and 48 h.

2.5. MTT assay & cell line maintenance

HCT-116 cancer cells (colon cancer) have been cultured in a 10% supplemented DMEM with heat-inactivated PBS and 50 μg/ml of penicillin at 37 °C within a 5% CO_2 atmosphere. Thereafter, the cells were seeded in the 96-well plates at a density of 3×10^3 cells per well in a complete DMEM medium for 24 h. Fe_3O_4/MSNs-NH_2, Fe_3O_4/MSNs-NH_2@OXA, and free OXA were added to the medium in the order of their appearances. Subsequent to being incubated for 48 h, the MTT solution (5 mg/mL PBS, 25 μL per well) was added to have the samples incubated for 4 h. The obtained results of IC_{50} values have been based on three independent experiments.

2.6. Statistical analysis

We have presented the gathered Data as the mean value ± standard deviation (SD). In addition, one-way ANOVA with post hoc test has been

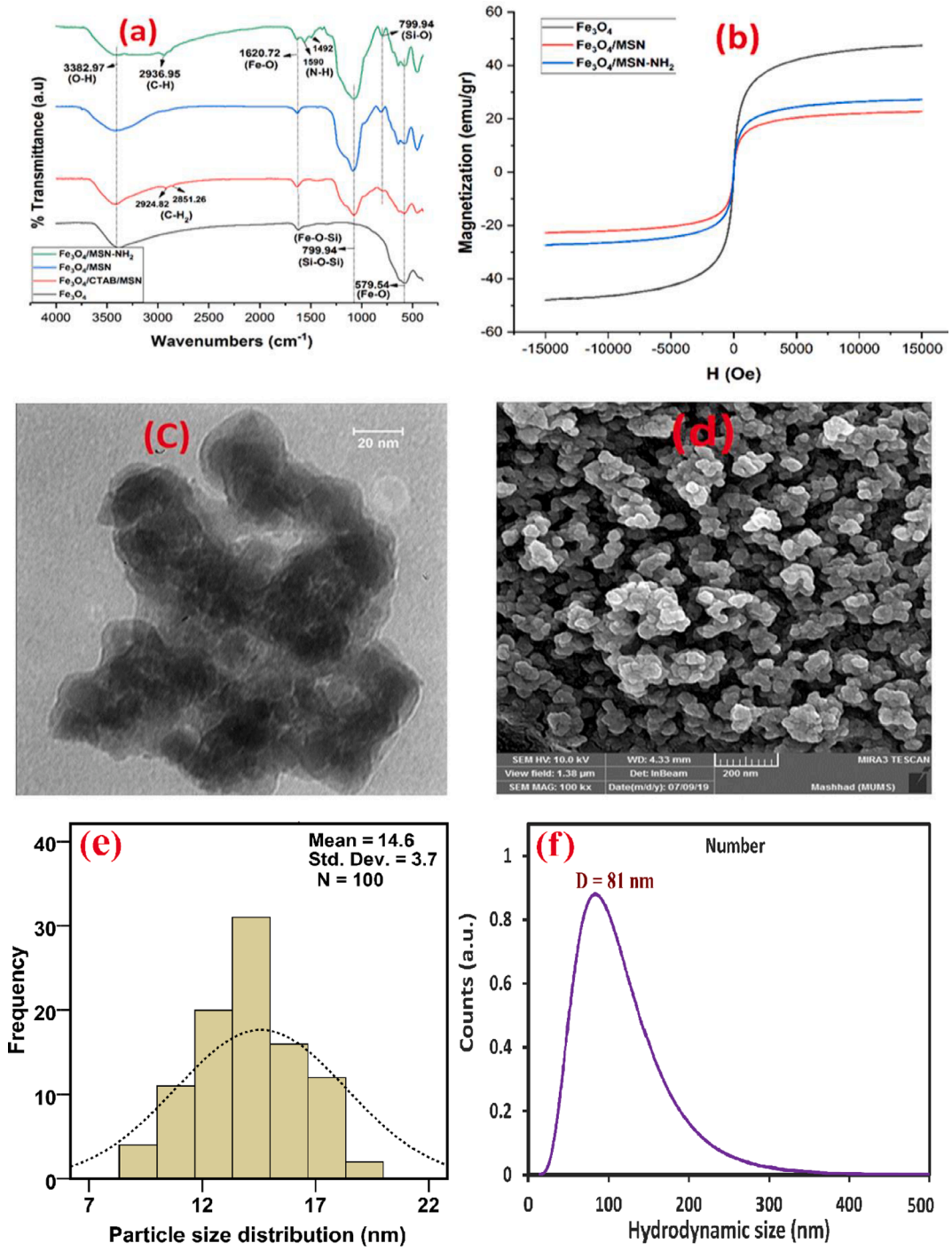

Fig. 2. a) FT-IR spectroscopy, b) VSM, c) TEM, d) FE-SEM, e) PSA curve, and f) DLS curve of nanoparticles.

used for calculating the statistical significance, while $P < 0.05$ had been considered statistically significant.

3. Result and discussion

3.1. Preparation and characterization of Fe_3O_4/MSNs-NH_2

The functionalized NCs have been prepared through a three-step process. For this purpose, Fe_3O_4 NPs have been synthesized and encapsulated by MSNs to reduce the toxicity of Fe_3O_4 and also prepare a magnetic nanocarrier. Then, the surface of MSNa has been modified by involving the NH_2-bonding in order to provide an affordable porosity for OXA. We have analyzed the as-prepared Fe_3O_4/MSNs-NH_2 by the means of FT-IR spectroscopy, VSM, TEM, and FE-SEM microscopy. According to FT-IR patterns (Fig. 2**a**), the formation of Fe_3O_4 (579.54, 1620.72 cm^{-1}) and MSNs (1077.1, 799.94 cm^{-1}) has occurred subsequent to the synthesizing processes, while the disappearing of 2924.82 and 2851.26 cm^{-1} peaks had confirmed the complete removal of CTAB from their structure after the calcination procedure [47,48]. Moreover, we have detected the signs of NH_2-bonding throughout 1590, 1492 (N-H), and 2936.95 cm^{-1} (C-H) peaks [49,50]. This work has provided exclusive data about the magnetic properties of NPs for each of the three steps of synthesizing process in Fig. 2**b** and accordingly, the NPs have had an optimal magnetization subsequent to being produced and modified. As it

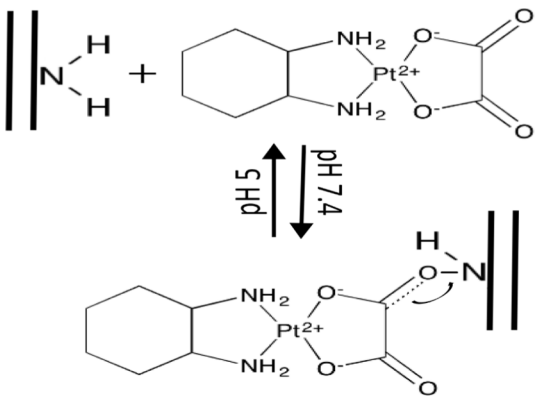

Fig. 3. Suggested schematic of the specific interaction between OXA-molecules and NH_2-bonding.

Table 1
Physical properties of nanoparticles.

Features	Fe_3O_4 NPs	Fe_3O_4/ MSN	Fe_3O_4/MSN/ NH_2
Zeta potential (mV) at pH 7.4 & water solvent.	−5.5	−19.66	+18.66
Average particle size (nm)	16	70	81
Polydispersity Index (PDI)	0.06	0.195	0.065
BET Surface area ($m^2.g^{-1}$)	70	371	316
Pore size (nm)	–	2.6	2.6
Pore volume ($cm^3.g^{-1}$)	–	0.404	0.344

can be observed through the TEM images (Fig. 2**c**), these NCs are capable of attracting more drugs and performing an increased drug loading due to containing a matrix-structure. This kind of structure (matrix) usually have been formed from smaller NPs so we introduced an agglomerated particle as one nanocarrier. What's more, in the biological system the NPs won't be able to work one by one, so it is a pivotal issue to consider the real properties of the prepared system to design a practical system. DLS analyze (Fig. 3**f**) have demonstrated the average size of final NCs at about 80 nm, while the TEM images and particle size distribution (Fig. 3**e**) have revealed that every single nanocarrier was about just 14 nm. Besides, the obtained FE-SEM image (Fig. 2**d**) has exhibited the dispersity and well-formation of NPs in the circle, which had also confirmed the matrix structure of NCs [51,52]. Furthermore, the potential properties of Fe_3O_4/MSNs-NH_2 for performing drug delivery has been affirmed through their physical features (Table 1), since their final size and PDI (81 nm, 0.065) have displayed their dispersity and compatibility in physiological situations. On the other hand, their surface area and pour diameter (371 $m^2.g^{-1}$, 26 nm) have been comparably applicable for achieving high percentages in drug loading as well. It had been also considerable that the zeta potential of final NCs (Fe_3O_4/MSN-NH_2) have been risen to around 19 mV and resulted in increasing their stability towards the highest level.

3.2. Loading capacity

The loading capacity of OXA has been measured by analyzing the ICP-OES spectra of supernatant fluid and for this purpose, 1 mL of free-OXA has been assessed for the existence of Pt elements since this method can only measure elements. Thereafter, the final solution, which had lacked the presence of NPs, has been evaluated through ICP-OES in regards to Pt elements measurement. The next steps have included investigating the OXA concentration by related molecular weight formula and calculating the amount of loaded drug by using the following formula (**Eq. 1**).

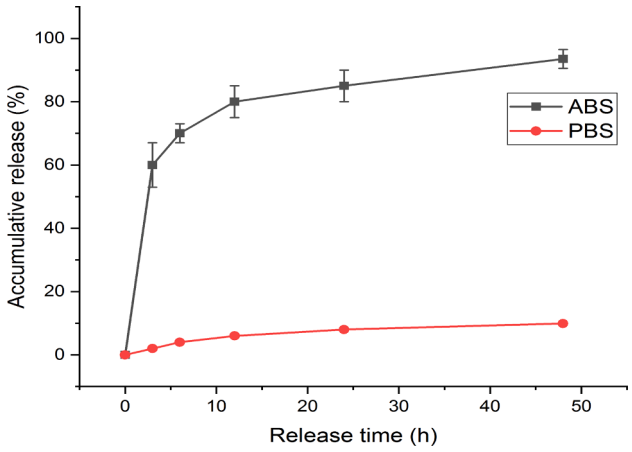

Fig. 4. The release profile of Fe_3O_4/MSNs-NH_2@OXA in the ABS and PBS.

$$Drug-loaded\% = \frac{totaldrug - loaded}{totaldrug - addedinitially} \times 100 (1)$$

The unmodified Fe_3O_4 MSN has been capable of absorbing only 18.5% of OXA under saturated loading conditions whereas according to the loading results, the Fe_3O_4/MSNs that had been functionalized with APTES have displayed an excellent absorption (55%). The occurrence of this increase in OXA loading capacity can be ascribed not only to the turning surface charge from negative to positive but also to the notable dispersity that had been caused by NH_2

-bonding. Another possible causing of raising drug-loaded might be related to a specific interaction between OXA and NH_2-bonded on the nanocarrier surface and pores. Moreover, regarding Fig. 3 there must be a bonding between O (form OXA) and N (from NH_2) which had been created in the natural pH via the protonate-deprotonate process and have made a high percentage of drug loading. We have also considered the assistance of OXA structure in facilitating an increase in the loading percentage since the particular structure and small size of OXA-molecules can be efficient in penetrating and passing through the porous structure of Fe_3O_4/MSNs-NH_2.

3.3. pH-responsive drug release and kinetic-release study

We have included samples with pH of 5.0 and pH of 7.4 in both cancer cells and human blood conditions for evaluating the pH-responsive release of Fe_3O_4/MSNs-NH_2@OXA. The amount of drug release has been investigated by the application of ICP-OES after 3, 6, 12, 24, and 48 h. According to Fig. 4, Fe_3O_4/MSNs-NH_2@OXA has exhibited more than 93% of drugs release after two days in cancer cells acidity situation, whereas in natural conditions, this value has reached under 10%. In regards to the case of cancer cells (pH of 5.0), the release profile had been required to be divide into two parts, before and after 3 h. In the first 3 h, we have observed a burst release (60%) while the remaining 40% of the drug were released over the next two days. The initial release probably related to NH_2-groups-protonate when drug-loaded NCs exposed to acidity cell-cancer circumstances. The suggested release process can be seen from Fig. 3. The second sustained release profile owing to leaving OXA-molecules the NCs' porosity.

As it is known a burst release is not considered suitable for nanomaterials, however, this model of release-profile is promising since it can prevent the immediate growth of cell cancers and maintain a sustained release until completing their destruction. On the other hand, there has not been any release (10% is negligible) detected in human blood situation (natural acidity).

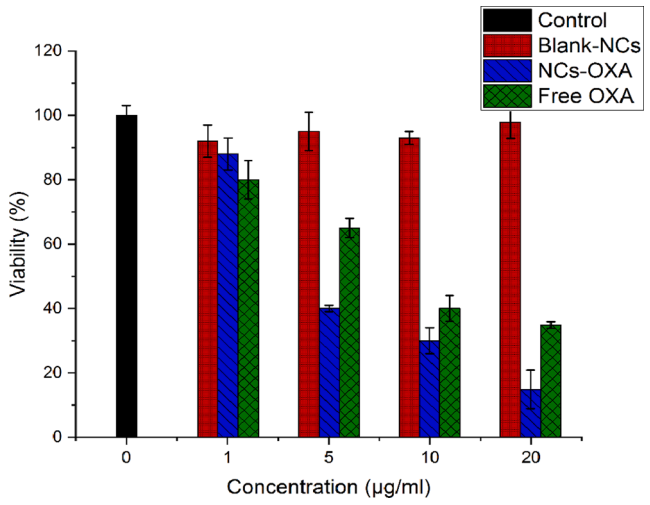

Fig. 5. Cell viability of control cells, Fe_3O_4/MSNs-NH_2, Fe_3O_4/MSNs-NH_2@OXA, and free OXA after 48 h.

3.4. MTT assay and cytotoxicity

The in vitro cytotoxicity of Fe_3O_4/MSNs-NH_2, Fe_3O_4/MSNs-NH_2@OXA, and free OXA has been evaluated by the means of MTT assay [53]. Briefly, Fe_3O_4/MSNs-NH_2, Fe_3O_4/MSNs-NH_2@OXA, and free OXA have been added to the 96-well plates and incubated with HCT-116 for 48 h, which had been followed by the addition of 20 mL of MTT (0.5 mg/mL) to the PBS solution. According to the represented curves in Fig. 5, we have observed a considerable decrease in the viability of HCT-116 against the increasing concentration of Fe_3O_4/MSNs-NH_2@OXA, which had been divided into two sections. However, the decrease recorded below 5 μg/mL has been quite notable, which had been probably caused by the instant release (the first part of the release profile) of OXA from Fe_3O_4/MSNs-NH_2@OXA. In conformity with the MTT results, the IC_{50} values of free OXA and Fe_3O_4/MSNs-NH_2@OXA subsequent to 48 h of incubation have been measured to be 7.5 and 3.2 μg/mL, respectively. The increase of uptake probable owing to an interaction between NH_2 and CD44-protein of the cell cancer and also the cationic NPs might have had special penetrating into the HCT116 cells in the comparing of anionic systems.

4. Conclusion

In this work, a novel version of drug-nanocarrier has been introduced for being applied in colon cancer treatment. The NCs have specialized over half (55%) of their capacity in the case of OXA and exhibited the highest drug loading percentage due to certain features including the structure of OXA (Fig. 1), converting surface potential into positive charges (+18.66 mV), well-dispersity of NCs (PDI: 0.065), specific interaction between OXA and NH_2, pore size, and volume (2.6 nm, 0.344 m^3. g^{-1}). However, the release profile of cell cancer and endocytosis condition (pH: 5.0) has been divided into two stages including the initial 60% of burst release that prevents the immediate growth of cell cancer and the second 40% of instant release, which is maintained for two days to complete the destruction of the cells. We have also detected an increase in the efficacy of NCs-OXA that had been twice as that of the Free drug (NCs-OXA IC_{50}: 3.2 μg/mL, Free OXA IC_{50}: 7.5 μg/mL), which is probably associated with the CD44-mediated endocytosis via NH_2-bonding. Furthermore, once the NCs-OXA had penetrated into the cell cancers, the NH_2-groups have created an interaction with the CD-44 receptors to increase the cytotoxicity of NCs-OXA.

Declaration of Competing Interest

The authors declare that they have no known competing financial interests or personal relationships that could have appeared to influence the work reported in this paper.

Acknowledgements

The authors gratefully acknowledge the technical support for this work provided by Ferdowsi University of Mashhad and Mashhad University of Medical Sciences based on the M. Sc thesis of Hamed Tabasi.

References

[1] H. Meng, W.X. Mai, H. Zhang, M. Xue, T. Xia, S. Lin, X. Wang, Y. Zhao, Z. Ji, J. I. Zink, A.E. Nel, Codelivery of an Optimal Drug/siRNA Combination Using Mesoporous Silica Nanoparticles To Overcome Drug Resistance in Breast Cancer in Vitro and in Vivo, ACS Nano 7 (2013) 994–1005.
[2] X. Ma, Q. Qu, Y. Zhao, Targeted delivery of 5-aminolevulinic acid by multifunctional hollow mesoporous silica nanoparticles for photodynamic skin cancer therapy, ACS Appl. Mater. Interfaces 7 (2015) 10671–10676.
[3] Q. He, J. Shi, F. Chen, M. Zhu, L. Zhang, An anticancer drug delivery system based on surfactant-templated mesoporous silica nanoparticles, Biomaterials 31 (2010) 3335–3346.
[4] A.V. Tran, K. Shim, T.T. Vo Thi, J.K. Kook, S.S.A. An, S.W. Lee, Targeted and controlled drug delivery by multifunctional mesoporous silica nanoparticles with internal fluorescent conjugates and external polydopamine and graphene oxide layers, Acta Biomater. 74 (2018) 397–413.
[5] H. He, H. Xiao, H. Kuang, Z. Xie, X. Chen, X. Jing, Y. Huang, Synthesis of mesoporous silica nanoparticle–oxaliplatin conjugates for improved anticancer drug delivery, Colloids Surf., B 117 (2014) 75–81.
[6] S. Sanchez-Salcedo, M. Vallet-Regí, S.A. Shahin, C.A. Glackin, J.I. Zink, Mesoporous core-shell silica nanoparticles with anti-fouling properties for ovarian cancer therapy, Chem. Eng. J. 340 (2018) 114–124.
[7] C. Chen, W. Sun, X. Wang, Y. Wang, P. Wang, pH-responsive nanoreservoirs based on hyaluronic acid end-capped mesoporous silica nanoparticles for targeted drug delivery, Int. J. Biol. Macromol. 111 (2018) 1106–1115.
[8] S.H. Wu, C.Y. Mou, H.P. Lin, Synthesis of mesoporous silica nanoparticles, Chem. Soc. Rev. 42 (2013) 3862–3875.
[9] A. Bitar, J. Vega-Chacón, Z. Lgourna, H. Fessi, M. Jafelicci, A. Elaissari, Submicron silica shell–magnetic core preparation and characterization, Colloids Surf., A 537 (2018) 318–324.
[10] W. Sheng, W. Wei, J. Li, X. Qi, G. Zuo, Q. Chen, X. Pan, W. Dong, Amine-functionalized magnetic mesoporous silica nanoparticles for DNA separation, Appl. Surf. Sci. 387 (2016) 1116–1124.
[11] M. Alghuthaymi, Magnetic-silica nanoshell for extraction of fungal genomic DNA from Rhizopus oryzae, Biointerface Res. Appl. Chem. 10 (2020) 4972–4976.
[12] A.H.F. Lee, S.F. Gessert, Y. Chen, N.V. Sergeev, B. Haghiri, Preparation of iron oxide silica particles for Zika viral RNA extraction, Heliyon 4 (2018).
[13] L.N. Zhang, M. Zhang, L.B. Liu, Y.Q. Wang, J. Zheng, J.L. Xu, Carbon-supported Ni and MoO_2 nanoparticles with Fe_3O_4 cores as a protein adsorbent, New J. Chem. 44 (2020) 15396–15402.
[14] S. Shi, W.T. Zhang, H.F. Wu, Y.C. Li, X.Y. Ren, M. Li, J. Liu, J. Sun, T.L. Yue, J. L. Wang, In Situ Cascade Derivation toward a Hierarchical Layered Double Hydroxide Magnetic Absorbent for High-Performance Protein Separation, ACS Sustain. Chem. Eng. 8 (2020) 4966–4974.
[15] S. Amornwutiroj, P. Manpetch, W. Singhapong, P. Srinophakun, A. Jaroenworaluck, Controllable synthesis of mesoporous magnetite/activated carbon composites as efficient adsorbents for hexavalent chromium removal, J. Dispersion Sci. Technol. 41 (2020) 1427–1444.
[16] F. Wang, Y.K. Sun, X.Z. Guo, D.Y. Li, H. Yang, Preparation and graft modification of hierarchically porous ferriferrous oxide for heavy metal ions adsorption, J. Sol-Gel Sci. Technol. 96 (2020) 360–369.
[17] T. Nawaz, S. Zulfiqar, M.I. Sarwar, M. Iqbal, Synthesis of diglycolic acid functionalized core-shell silica coated Fe_3O_4 nanomaterials for magnetic extraction of Pb(II) and Cr(VI) ions, Sci. Rep. 10 (2020) 13.
[18] R. Ladj, A. Bitar, M. Eissa, Y. Mugnier, R. Le Dantec, H. Fessi, A. Elaissari, Individual inorganic nanoparticles: preparation, functionalization and in vitro biomedical diagnostic applications, J. Mater. Chem. B 1 (2013) 1381–1396.
[19] R. Jin, B. Lin, D. Li, H. Ai, Superparamagnetic iron oxide nanoparticles for MR imaging and therapy: design considerations and clinical applications, Curr. Opin. Pharmacol. 18 (2014) 18–27.
[20] V. Patsula, L. Kosinova, M. Lovric, L. Ferhatovic Hamzic, M. Rabyk, R. Konefal, A. Paruzel, M. Slouf, V. Herynek, S. Gajovic, D. Horak, Superparamagnetic Fe_3O_4 Nanoparticles: Synthesis by Thermal Decomposition of Iron(III) Glucuronate and Application in Magnetic Resonance Imaging, ACS Appl. Mater. Interfaces 8 (2016) 7238–7247.
[21] Z. Hedayatnasab, A. Dabbagh, F. Abnisa, W. Daud, Synthesis and in-vitro characterization of superparamagnetic iron oxide nanoparticles using a sole precursor for hyperthermia therapy, Mater. Res. Bull. 132 (2020) 10.

[22] B.P. Meneses-Brassea, C.M. Cyr, I. Martinez, C.E. Botez, A.A. El-Gendy, Facile synthesis of superparamagnetic Fe3O4 nanoparticles at therapeutic temperature range for magnetic hyperthermia therapy, J. Nanopart. Res. 22 (2020) 6.
[23] E. Yu, I. Galiana, R. Martinez-Manez, P. Stroeve, M.D. Marcos, E. Aznar, F. Sancenon, J.R. Murguia, P. Amoros, Poly(N-isopropylacrylamide)-gated Fe_3O_4/SiO_2 core shell nanoparticles with expanded mesoporous structures for the temperature triggered release of lysozyme, Colloids and surfaces B, Biointerfaces 135 (2015) 652–660.
[24] F. Yang, W. Xiao, X. Ma, R. Huang, R. Yu, G. Li, X. Huang, C. Chen, P. Ding, Optimization of a novel chelerythrine-loaded magnetic Fe_3O_4 /chitosan alpha-ketoglutaric acid system and evaluation of its anti-tumour activities, J. Pharm. Pharmacol. 68 (2016) 1030–1040.
[25] A.O. Baskakov, et al., Magnetic and interface properties of the core-shell Fe3O4/Au nanocomposites, Appl. Surf. Sci. 422 (2017) 638–644.
[26] M.A. Rabbi, M.M. Rahman, H. Minami, N. Yamashita, M.R. Habib, H. Ahmad, Magnetically responsive antibacterial nanocrystalline jute cellulose nanocomposites with moderate catalytic activity, Carbohydr. Polym. 251 (2021), 117024.
[27] S. Mapukata, N. Nwahara, T. Nyokong, The photodynamic antimicrobial chemotherapy of Stapphylococcus aureus using an asymmetrical zinc phthalocyanine conjugated to silver and iron oxide based nanoparticles, J. Photochem. Photobiol. A-Chem. 402 (2020) 15.
[28] N. Abutaha, A. Hezam, F.A. Almekhlafi, A.M.N. Saeed, K. Namratha, K. Byrappa, Rational design of Ag-ZnO-Fe_3O_4 nanocomposite with promising antimicrobial activity under LED light illumination, Appl. Surf. Sci. 527 (2020) 8.
[29] M.A. Rabbi, M.M. Rahman, H. Minami, N. Yamashita, M.R. Habib, H. Ahmad, Magnetically responsive antibacterial nanocrystalline jute cellulose nanocomposites with moderate catalytic activity, Carbohydr. Polym. 251 (2021) 11.
[30] P. Senthilkumar, S. Babu, V. Jaishree, K.J. Stephen, G. Yaswant, D. Kumar, N. S. Nair, Solvothermal-assisted green synthesis of hybrid Chi-Fe_3O_4 nanocomposites: a potential antibacterial and antibiofilm material, IET Nanobiotechnol. 14 (2020) 714–721.
[31] J.A.A. Abdullah, L.S. Eddine, B. Abderrhmane, M. Alonso-Gonzalez, A. Guerrero, A. Romero, Green synthesis and characterization of iron oxide nanoparticles by pheonix dactylifera leaf extract and evaluation of their antioxidant activity, Sustain. Chem. Pharm. 17 (2020) 7.
[32] A. Bouafia, S.E. Laouini, A. Khelef, M.L. Tedjani, F. Guemari, Effect of Ferric Chloride Concentration on the Type of Magnetite (Fe3O4) Nanoparticles Biosynthesized by Aqueous Leaves Extract of Artemisia and Assessment of Their Antioxidant Activities, J. Clust. Sci., 9.
[33] M. Ghoorchibeigi, K. Larijani, P.A. Azar, K. Zare, I. Mehregan, ZnO/Fe(3)O(4) nanoparticles promoted green synthesis of pyrazolo pyrimidinones: Study of antioxidant activity, J. Heterocycl. Chem. 57 (2020) 3612–3621.
[34] S.M. Taimoory, A. Rahdar, M. Aliahmad, F. Sadeghfar, M.R. Hajinezhad, M. Jahantigh, P. Shahbazi, J.F. Trant, The synthesis and characterization of a magnetite nanoparticle with potent antibacterial activity and low mammalian toxicity, J. Mol. Liq. 265 (2018) 96–104.
[35] A. Taufiq, H.N. Ulya, C.I. Yogihati, N. Sunaryono, N. Mufti Hidayat, S. Masruroh, T. Ishida Soda, Effects of ZnO nanoparticles on the antifungal performance of Fe_3O_4/ZnO nanocomposites prepared from natural sand, Adv. Nat. Sci.-Nanosci Nanotechnol 11 (2020) 10.
[36] M.H. Kahsay, N. Belachew, A. Tadesse, K. Basavaiah, Magnetite nanoparticle decorated reduced graphene oxide for adsorptive removal of crystal violet and antifungal activities, RSC Adv. 10 (2020) 34916–34927.
[37] A.A. Hernandez-Hernandez, G. Aguirre-alvarez, R. Carino-Cortes, L.H. Mendoza-Huizar, R. Jimenez-Alvarado, Iron oxide nanoparticles: synthesis, functionalization, and applications in diagnosis and treatment of cancer, Chem. Pap. 74 (2020) 3809–3824.
[38] A. Bitar, N.M. Ahmad, H. Fessi, A. Elaissari, Silica-based nanoparticles for biomedical applications, Drug Discovery Today 17 (2012) 1147–1154.
[39] R. Ladj, A. Bitar, M.M. Eissa, H. Fessi, Y. Mugnier, R. Le Dantec, A. Elaissari, Polymer encapsulation of inorganic nanoparticles for biomedical applications, Int. J. Pharm. 458 (2013) 230–241.
[40] N. Graf, S.J. Lippard, Redox activation of metal-based prodrugs as a strategy for drug delivery, Adv. Drug Deliv. Rev. 64 (2012) 993–1004.
[41] S.J. Berners-Price, Activating platinum anticancer complexes with visible light, Angew. Chem. 50 (2011) 804–805.
[42] C. Liang, H. Wang, M. Zhang, W. Cheng, Z. Li, J. Nie, G. Liu, D. Lian, Z. Xie, L. Huang, X. Zeng, Self-controlled release of Oxaliplatin prodrug from d-α-tocopheryl polyethylene glycol 1000 succinate (TPGS) functionalized mesoporous silica nanoparticles for cancer therapy, J. Colloid Interface Sci. 525 (2018) 1–10.
[43] H. Xiao, D. Zhou, S. Liu, Y. Zheng, Y. Huang, X. Jing, A complex of cyclohexane-1,2-diaminoplatinum with an amphiphilic biodegradable polymer with pendant carboxyl groups, Acta Biomater. 8 (2012) 1859–1868.
[44] J. Zhang, Y. Sun, B. Tian, K. Li, L. Wang, Y. Liang, J. Han, Multifunctional mesoporous silica nanoparticles modified with tumor-shedable hyaluronic acid as carriers for doxorubicin, Colloids and surfaces, B, Biointerfaces 144 (2016) 293–302.
[45] Y. Wang, Q. Zhao, N. Han, L. Bai, J. Li, J. Liu, E. Che, L. Hu, Q. Zhang, T. Jiang, S. Wang, Mesoporous silica nanoparticles in drug delivery and biomedical applications, Nanomed. Nanotechnol. Biol. Med. 11 (2015) 313–327.
[46] Y. Wang, Y. Cui, Y. Zhao, B. He, X. Shi, D. Di, Q. Zhang, S. Wang, Fluorescent carbon dot-gated multifunctional mesoporous silica nanocarriers for redox/enzyme dual-responsive targeted and controlled drug delivery and real-time bioimaging, European journal of pharmaceutics and biopharmaceutics : official journal of Arbeitsgemeinschaft fur Pharmazeutische, Verfahrenstechnik e.V 117 (2017) 105–115.
[47] A. Badri, I. Alvarez-Serrano, M. Luisa López, M. Ben Amara, Sol-gel synthesis, magnetic and methylene blue adsorption properties of lamellar iron monophosphate $KMgFe(PO_4)_2$, Inorg. Chem. Commun. 121 (2020), 108217.
[48] S. Ghazal, A. Akbari, H.A. Hosseini, Z. Sabouri, F. Forouzanfar, M. Khatami, M. Darroudi, Sol-gel biosynthesis of nickel oxide nanoparticles using Cydonia oblonga extract and evaluation of their cytotoxicity and photocatalytic activities, J. Mol. Struct. 1217 (2020), 128378.
[49] M. Abboud, S. Youssef, J. Podlecki, R. Habchi, G. Germanos, A. Foucaran, Superparamagnetic Fe_3O_4 nanoparticles, synthesis and surface modification, Mater. Sci. Semicond. Process. 39 (2015) 641–648.
[50] K. Onar, M.E. Yakinci, Synthesis of Fe_3O_4 nanoparticles for biomedical applications, J. Phys. Conf. Ser. 667 (2016), 012005.
[51] A. Akbari, Z. Sabouri, H.A. Hosseini, A. Hashemzadeh, M. Khatami, M. Darroudi, Effect of nickel oxide nanoparticles as a photocatalyst in dyes degradation and evaluation of effective parameters in their removal from aqueous environments, Inorg. Chem. Commun. 115 (2020), 107867.
[52] Z. Sabouri, A. Akbari, H.A. Hosseini, M. Khatami, M. Darroudi, Egg white-mediated green synthesis of NiO nanoparticles and study of their cytotoxicity and photocatalytic activity, Polyhedron 114351 (2020).
[53] Z. Sabouri, A. Akbari, H.A. Hosseini, M. Khatami, M. Darroudi, Tragacanth-mediate synthesis of NiO nanosheets for cytotoxicity and photocatalytic degradation of organic dyes, Bioprocess Biosyst. Eng. (2020).